LCL Filter Design for Three Phase AC-DC Converters Considering Semiconductor Modules and Magnetics Components Performance

Stecca, Marco; Soeiro, Thiago Batista; Ramirez Elizondo, Laura; Bauer, Pavol; Palensky, Peter

LCL Filter Design for Three Phase AC-DC Converters Considering Semiconductor Modules and Magnetics Components Performance

Marco Stecca, Thiago Batista Soeiro, Laura Ramirez Elizondo, Pavol Bauer, and Peter Palensky
DELFT UNIVERSITY OF TECHNOLOGY
Delft, The Netherlandsy
Phone: +31 (0) 15-278-9042
Email: m.stecca@tudelft.nl

Keywords

≪Voltage Source Converter (VSC)≫, ≪Passive filter≫.

Abstract

LCL filters are commonly adopted to attenuate the current harmonics produced by Pulse Width Modulation (PWM) Voltage Source Converters (VSC). Due to the nature of LCL filters, several combinations of L and C can deliver the attenuation required by the standards. The optimal configuration is generally evaluated, considering power density, costs, and filter efficiency. This paper shows that semiconductor efficiency should also be considered as an important design variable. It is shown that the AC ripple across the converter side inductor can reduce, to a certain extent, the overall semiconductor losses, when commercial IGBTs and the respective anti-parallel diodes are used. Reduced losses have benefits in terms of semiconductor module lifetime, chip area and cost reduction, and simplification of cooling requirements. Higher AC ripple, however, negatively affect the filter losses. Nonetheless, inductive components are typically much less critical in terms of losses dissipation and lifetime than semiconductors.

Introduction

Voltage Source Converters (VSCs) are used to interface, among others, renewable energy-based generators, battery energy storage systems, and electric motors with the electrical network [1]. Pulse Width Modulation (PWM) techniques for the control of VSCs, intrinsically generate harmonics in the AC output terminal. However, the connection to the main network requires compliance to several standards that regulate, i.e., the current harmonic limits [2]. In this context, LCL filters are widely adopted for the reduction of the high order harmonics. The design of LCL filters has already been widely treated in the literature. Methods for defining the boundary values of the filter components and their design have been proposed in [3, 4]. Due to the nature of LCL filters, a specific harmonic attenuation can be obtained with several values of the inductive and capacitive components; therefore other variables, such as cost, weight, volume and power losses, can play a significant role in the selection of the LCL filter optimal parameters [4]. Furthermore, also the amplitude of the ripple current flowing in the converter is defined by the filter parameters. In medium-high power systems, the LCL filter assumes relevant weight and size, becoming a key design variable; hence, various studies include efficiency and power density as optimization criterion [5, 6]. On the other hand, in previous studies, the direct influence of the AC ripple amplitude, driven by the selection of the LCL parameters, in the power losses of the semiconductor modules, is often neglected. Therefore, this paper will address the influence of the AC current ripple on the semiconductor modules efficiency of VSCs when designing its LCL filter.

In this paper, a three phase three-wire 100 kW DC-AC converter, as shown in Fig. 1, is taken as a case study. The filter parameters are analytically calculated considering the relevant standards, such as the IEEE 519-2014 [2], and the losses in the passive components are evaluated through well-established
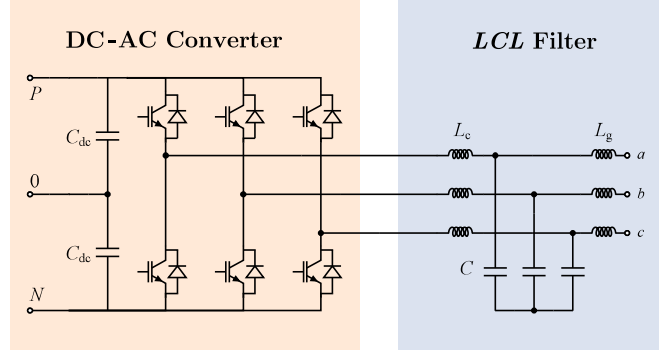
Fig. 1: Three-wire Voltage Source Converter with LCL output filter

methods in literature [5, 7, 8]. The resulting possible filter designs are benchmarked in terms of weight, size, and power losses. In this respect, a particular focus on the impact of the AC ripple on the semiconductors' losses is given. It is shown that, for the selected commercial semiconductors IGBT-Diode modules, the AC ripple can reduce switching losses, increasing the lifetime of the modules and decreasing the required cooling resources. By contrast, the AC ripple has a negative impact on the filter losses. Thereby a trade-off between semiconductor and filter efficiency has to be made. In this respect, it has to be considered that inductive components are not as demanding as the semiconductor modules in terms of cooling, thermal management, and losses dissipation. Consequently, selecting the LCL filter parameters to have the minimum semiconductor losses can lead to lower cooling efforts and lower semiconductor stress at the expense of a slight reduction of the LCL filter overall efficiency.

Filter parameter selection

In grid-connected VSCs, LCL filters are widely used to suppress the injected current harmonics generated by the converter AC output voltages. According to the IEEE 519-2014 standard, high frequency odd current harmonics ($h > 35$) need to be contained to less than 0.3% of the nominal line frequency current, I_n, and even harmonics to 0.075% of it [2]. The amplitude of the hth current harmonic produced by the converters can be calculated as the ratio between the peak harmonic voltage and the filter impedance at that specific frequency. The voltage harmonic spectrum for the three-wire two-level VSC operated with PWM modulation can be analytically calculated through double Fourier integration [9]. The first relevant harmonic is the sideband $f_s - 2f_g$, thus, starting from this harmonic, the filter needs to be able to provide the minimum required attenuation that guarantees the compliance to the standards. The -60 dB slope of the filter transfer function will effectively further attenuate the higher-order harmonics. Once obtained the harmonic voltage amplitude, if $f_s - 2f_g > 35f_g$, the required attenuation, according to the IEEE 519 standard, can be found through equation (1):

$$Att_{\text{IEEE}-519} = 0.003 \frac{P_{\text{nom}}}{\sqrt{3}V_{\text{ll}}V_{1,-2}}. \tag{1}$$

where P_{nom} is the nominal power of the converter, V_{ll} is the line-to-line AC voltage, and $V_{1,-2}$ is the $f_s - 2f_g$ sideband harmonic voltage. The transfer function of a LCL filter is given by equation (2):

$$H(s) = \frac{\omega_{\text{res}}^2}{s\left(L_g + L_c\right)\left(s^2 + \omega_{\text{res}}^2\right)}, \tag{2}$$

where:

$$\omega_{\text{res}} = k_{\text{res}}\omega_s = \sqrt{\frac{L_c + L_g}{L_c L_g C}} \tag{3}$$

Parameter	P_{nom}	V_{dc}	$V_{\text{ac,ll}}$	f_s	k_{res}	f_g
Value	100 kW	900 V	400 V	8 kHz	0.35	50 Hz

and L_c and L_g are respectively the converter side and grid side inductances and C the capacitance of the filter, as indicated in Fig. 1. The resonance frequency of the filter needs to be carefully evaluated to avoid the amplification of the sideband harmonics and to guarantee control stability [10]. Knowing the attenuation required, as defined in Equation (1), and given the LCL filter transfer function, Equation (2), the minimum total inductance that guarantees standards' compliance can be found as:

$$L_{\text{tot,min}} = \frac{k_{\text{res}}^2 \omega_s^2}{\omega_h \left(\omega_h^2 - k_{\text{res}}^2 \omega_s^2 \right) Att_{\text{IEEE}-519}}.$$

(4)

The maximum value of L_{tot}, instead, is limited by the voltage drop across the filter. For S-PWM, Equation (5) gives the upper boundary [4]:

$$L_{\text{tot,max}} = \frac{\sqrt{\frac{V_{\text{dc}}^2}{8} - \frac{V_{\text{ll}}^2}{3}}}{2\pi f_c I_n}$$

(5)

As shown in Equation (2), the harmonic attenuation in the grid side current for a fixed filter resonance frequency is given by the sum of the converter side L_c and grid side L_g inductances. Additionally, the converter side inductance, for a fixed filter resonance frequency, defines the amplitude of the AC current ripple flowing through the semiconductors, since the transconductance $Y_{1,1} = i_1/v_1$ that defines the convert side current harmonics is expressed as:

$$Y_{11}(s) = \frac{s^2 + \omega_{\text{lc}}^2}{sL_c \left(s^2 + \omega_{\text{res}}^2 \right)},$$

(6)

where:

$$\omega_{\text{lc}} = \frac{1}{CL_c}.$$

(7)

The grid side inductance, L_g, can be found subtracting L_c from L_{tot}. Having the values of the inductances L_c and L_g and fixing the resonance frequency, the capacitance value is derived rearranging Equation (2). The maximum reactive power absorption at grid frequency gives the upper boundary for the capacitance value, usually limited to 5% the nominal power. The reactive power injected by the capacitor needs to be compensated by the converter, lowering its efficiency, especially at low partial loads.

Once defined the parameter boundaries, several possible designs for the LCL filter can be found by varying L_c. The feasible LCL parametric combinations, derived according to the parameters listed in Table I are plotted in Fig. 2. Increasing the value of L_c the peak current ripple decreases and as well L_g, since the L_{tot} is kept constant and equal to the minimum required value. To evaluate the impact of the AC ripple in the efficiency of the semiconductor and the LCL filter, several combinations of LCL parameters are selected and further designed. These are chosen to have linear variations of the AC ripple, and they are indicated in Fig. 2 by the vertical brown dashed lines. To compare the L_c, L_g and C combinations, it is necessary to analyze more in-depth the inductor design, and the power losses on the semiconductor modules, as presented in the following Sections.

Inductors design

As mentioned in the previous Section, to evaluate the performance of the LCL filter, it is necessary to design its components. The bulk of the losses in the LCL filter are usually found in the converter side
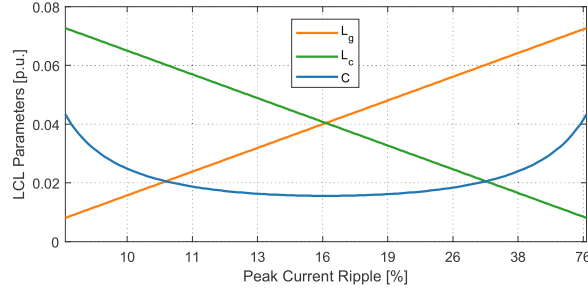
Fig. 2: LCL filter possible design for a grid connected VSC with the specifications listed in Table I.

inductor since the high frequency ripple will flow through it, affecting both high frequency winding losses and core losses. In this paper, the inductors are designed considering commercially available toroidal-shape cores from ChangSung [11]. Starting from the core material permeability μ, the mean magnetic path length $l[m]$ and the effective cross area section $A[m^2]$, the number of turns that give the required inductance $L[H]$ can be found as:

$$N = \sqrt{\frac{Ll}{0.4\mu\pi A 10^{-2}}}.\tag{8}$$

Then, the total winding length l_w can be found according to the number of turns N and the core material dimensions. The power losses in the inductors can be separated in winding losses, due to the skin and proximity effect, and core losses:

$$P_\mathrm{ind} = P_\mathrm{skin} + P_\mathrm{prox} + P_\mathrm{core}.\tag{9}$$

The skin effect losses are evaluated through:

$$P_\mathrm{skin} = l_\mathrm{w}R_\mathrm{ac}\hat{I}_\mathrm{hf}^2 + \frac{1}{2}l_\mathrm{w}R_\mathrm{dc}\hat{I}_\mathrm{ac}^2,\tag{10}$$

where $\hat{I}_\mathrm{hf}$ is the high frequency peak current, $\hat{I}_\mathrm{ac}$ the peak sinusoidal AC current, R_ac and R_dc are the AC and DC resistance of the windings, and δ the skin depth which are found according to the wire diameter d and its conductance σ:

$$R_\mathrm{dc} = \frac{4}{\sigma d^2 \pi},\tag{11}$$

$$\delta = \frac{1}{\sqrt{\pi\mu_0\sigma f}}.\tag{12}$$

The AC resistance of the inductor winding, instead, is calculated through the analytical approximation given by [7]:

$$R_\mathrm{ac} = R_\mathrm{dc}\frac{\gamma}{4\sqrt{2}}\left(\frac{\mathrm{ber}_0\gamma\mathrm{bei}_1\gamma - \mathrm{bei}_0\gamma\mathrm{ber}_1\gamma}{\mathrm{ber}_1^2\gamma + \mathrm{bei}_1^2\gamma} - \frac{\mathrm{bei}_0\gamma\mathrm{ber}_1\gamma - \mathrm{bei}_0\gamma\mathrm{bei}_1\gamma}{\mathrm{ber}_1^2\gamma + \mathrm{bei}_1^2\gamma}\right)\tag{13}$$

Table II: Specifications of the selected LCL filter designs and calculated power losses in the inductors at rated power.

Design #	L_g [μH]	L_c [μH]	C [μF]	Ripple [%]	Losses in L_c[W]	Losses in L_g[W]
1	370	41	86	9	96	69
2	74	337	53	42	80	50
3	41	370	86	76	122	65

with ber_r and bei_i the real and imaginary parts of the Kelvin function of the ith order, and γ defined as:

$$\gamma = \frac{d}{\sqrt{2}\delta}. \tag{14}$$

The proximity effect losses depend on the external magnetic field $\hat{H}_e$, derived following the approach of [12], and can be calculated as [5, 7]:

$$P_{\mathrm{prox}} = R_{\mathrm{dc}} G_R \hat{H}_e^2 \tag{15}$$

$$G_R = \frac{\gamma \pi^2 d^2}{2\sqrt{2}} \left(\frac{\mathrm{ber}_2 \gamma \mathrm{ber}_1 \gamma - \mathrm{ber}_2 \gamma \mathrm{bei}_1 \gamma}{\mathrm{ber}_0^2 \gamma + \mathrm{bei}_0^2 \gamma} + \frac{\mathrm{bei}_2 \gamma \mathrm{bei}_1 \gamma - \mathrm{bei}_2 \gamma \mathrm{ber}_1 \gamma}{\mathrm{ber}_0^2 \gamma + \mathrm{bei}_0^2 \gamma} \right) \tag{16}$$

Equations (10)-(16) are then applied for evaluating the winding losses caused by each current harmonic in which the current flowing through the inductor can be decomposed. Finally, the total winding losses are found through summing the contribution of each harmonics.

The core losses are calculated through the *improved Generalized Steinmetz Equation* (iGSE). For a triangular waveform the iGSE takes the following formulation [13]:

$$P_{\mathrm{core}} = k f_{\mathrm{s}} \left(\frac{2}{\pi^2} 4 f_{\mathrm{s}} \right)^{\alpha - 1} \hat{B}^\beta V_{\mathrm{core}} \tag{17}$$

$$k = \frac{k}{(2\pi)^{\alpha - 1} \int_0^{2\pi} |\cos\theta|^\alpha 2^{\beta - \alpha} d\theta} \tag{18}$$

where V_{core} is the core volume, k, α and β are the Steinmetz parameters derived from the core material, and $\hat{B}$ is the peak to peak flux density given in Equation (19) as a function of the peak to peak current ripple $I_{\mathrm{r,pp}}$ and the inductor geometry:

$$\hat{B} = \frac{L I_{\mathrm{r,pp}}}{2NA} \tag{19}$$

As previously mentioned, the *iGSE* estimates the core losses derived by a triangular shaped current. The total inductor core losses are then calculated summing the contribution of each triangular minor loop in which the switched current can be divided and averaging the total in the 50 Hz period.

Applying the method described through Equations (8) - (19) the power losses on the LCL filter inductors can be analytically calculated. This procedure is repeated varying the core diameter, the number of stacked elements, and the core material, according to the specifications of the commercially available toroidal Powder Core [11] to design the inductors of three possible LCL configurations, whose parame-
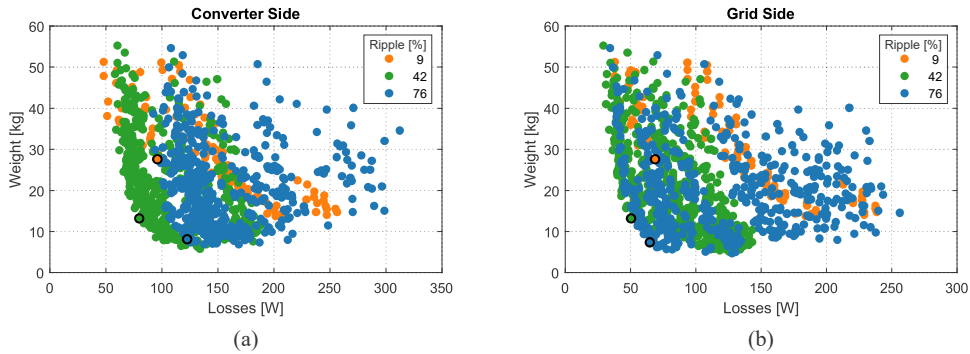

Fig. 3: L_{c} and L_{g} power losses and weight design space for different ripple amplitudes and so inductance value, according to the parameters of Table II. The selected designs are circled by a black line.
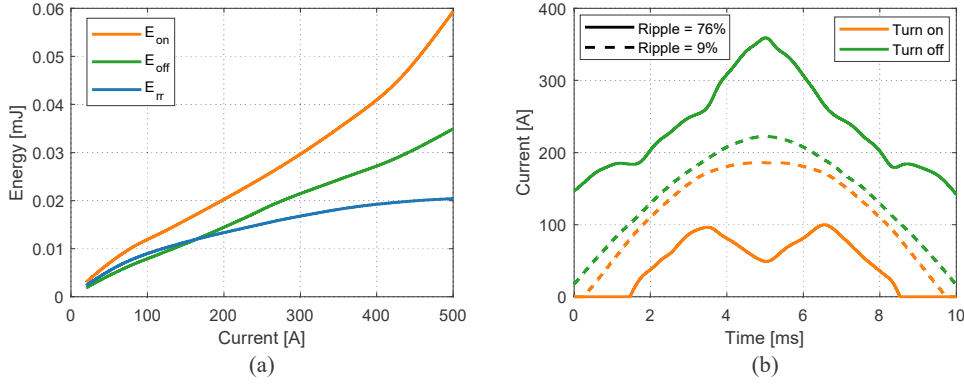
Fig. 4: (a) Semikron SKM400GB125D module switching characteristics from datasheet; and (b) turn on and turn off currents of the upper IGBT with different ripple amplitudes at rated power.

ters are specified in Table II. These three configurations lead to different AC current ripple values so that its influence on the system performance can be later estimated.

In Fig. 3 the losses and weight design space of L_c and L_g in these three configurations are plotted. The designs are checked for thermal compliance so that their maximum temperature does not exceed 150°C. Between all the feasible designs, the selected designs of L_c and L_g in the three configurations are highlighted by a black circle in Fig. 3. These are selected to be in the knee of the weight-losses Pareto front so that they exhibit the optimal trade-off between the two parameters.

Full system efficiency

The current flowing through the semiconductor modules consists of the sum of the fundamental 50 Hz current and the high frequency AC ripple. Given a specific current waveform, it is possible to derive conduction, P_c, and switching, P_s, power losses in the semiconductor, through equations (20)-(22).

$$P_{c,i} = v_i I_{\text{avg},i} + r_i I_{\text{rms},i}^2 \tag{20}$$

$$P_{s,IGBT} = \frac{f_s V_{dc}}{4\pi V_b} \int_{-\varphi}^{2\pi - \varphi} \left[E_{on}\left(I_g\right) + E_{off}\left(I_g\right) \right] dt \tag{21}$$

$$P_{s,Diode} = \frac{f_s V_{dc}}{4\pi V_b} \int_{-\varphi}^{2\pi - \varphi} E_{rr}\left(I_g\right) dt \tag{22}$$

v_i and r_i are the on state characteristics of the component i, from the semiconductor datasheet, φ the phase shift between the fundamental AC output voltage and current, V_{dc} the switching voltage, V_b the datasheet measured switching voltage, and $E_{on}(I_g)$, $E_{off}(I_g)$, and $E_{rr}(I_g)$ the switching energy functions, extracted from the semiconductor datasheet and plotted in Fig. 4(a). The commercially available Semikron IGBT-Diode half-bridge module SKM400GB125D, rated 1200V-300A, has been considered [14]. The conduction losses are marginally affected by the ripple since the average, and RMS value of the current through the semiconductor do not see significant variations. However, the IGBT turn-off current significantly increases. At the same time, the turn-on decreases, leading to soft switching at the beginning and the end of the half period, as indicated in Fig. 4(b). It is then expected an increase in the turn off losses and a decrease in the turn-on losses. These variations are also linked to the switching energy of the semiconductors modules. If the IGBTs are selected to have turn-off losses comparable lower to the sum of the turn-on and the reverse recovery of the diode, then it is expected an overall decrease in the switching losses when the AC ripple increases. The IGBT module SKM400GB125D has turn-on energy higher than turn off and reverse recovery energy; consequently, its performance will benefit from the AC ripple superimposition, as detailed in Fig. 5(a).

Fig. 5(b) displays the semiconductor module efficiency varying the converter output power for different peak values of the high frequency ripple, according to the LCL parameters described in Table II. What
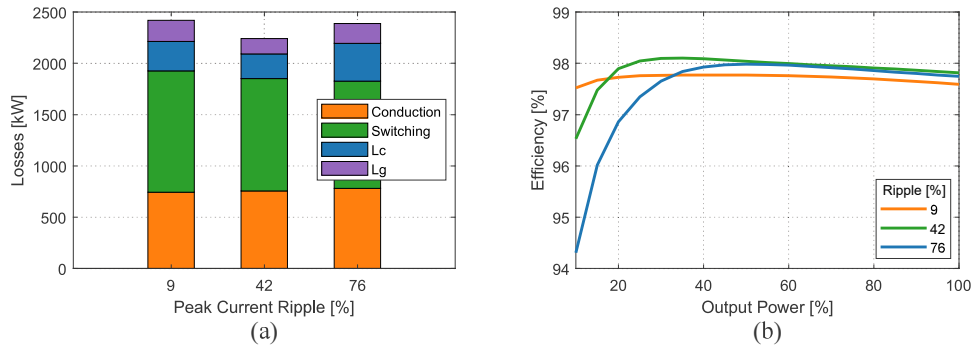
Fig. 5: (a) Semiconductor module and LCL filter losses breakdown at rated power; and (b) efficiency curves at partial load for the VSC employing the three selected LCL filter designs.

stands out from Fig. 5(b) is the fact that, for the selected IGBT module, a low ripple amplitude shows a relatively flat efficiency curve at partial loads with considerable benefits at low partial loads. However, for a high partial load operation, the high AC current ripple's superposition improves the overall system performances and reduces the semiconductor power losses.

In this context, the LCL filter parameters can also be designed according to the VSC's application requirements and mission profile, seeking to maximize the semiconductor module efficiency with the appropriate amplitude of the high frequency AC current ripple. The semiconductor modules can benefit in terms of lower losses from the AC ripple current. Lower losses translate in lower cooling requirements and less degradation of the switches due to junction temperature variations. However, the impact of the AC ripple is strongly related to the semiconductor switching characteristics. The LCL configuration that assures the best semiconductor performance has to be evaluated case by case.

Conclusions and future work

An analytical procedure for the LCL filter design and the evaluation of the filter and AC-DC converter efficiency based on well-established methods in literature have been presented. Following the proposed approach, it has been shown how the AC ripple affects not only the design and efficiency of the output filter but also the performances of the semiconductor modules. More in detail it has been shown that the AC ripple, until a certain extent, and depending on the output power of the AC-DC converter, can have a beneficial impact on the IGBT-Diode losses, leading to lower thermal stress of the semiconductors and reducing the requirements of the thermal management system. This, however, comes at the price of lower efficiency of the LCL filter. Future work will focus on extending the analysis, considering more broadly the converter operating conditions, i.e., reactive power generation. Experimental verification of the results will be performed to verify the models adopted.

References

[1] M. Stecca, L. Ramirez Elizondo, T. Batista Soeiro, P. Bauer, and P. Palensky, "A Comprehensive Review of the Integration of Battery Energy Storage Systems into Distribution Networks," *IEEE Open J. Ind. Electron. Soc.*, vol. 1, pp. 46–65, 2020.

[2] IEEE Standards Association, "IEEE Std. 519-2014. IEEE Recommended Practice and Requirements for Harmonic Control in Electric Power Systems," pp. 1–29, 2014.

[3] M. Liserre, F. Blaabjerg, and S. Hansen, "Design and control of an LCL-filter-based three-phase active rectifier," *IEEE Trans. Ind. Appl.*, vol. 41, no. 5, pp. 1281–1291, 2005.

[4] K. Jalili and S. Bernet, "Design of LCL filters of active-front-end two-level voltage-source converters," *IEEE Trans. Ind. Electron.*, vol. 56, no. 5, pp. 1674–1689, 2009.

[5] J. Mühlethaler, M. Schweizer, R. Blattmann, J. W. Kolar, and A. Ecklebe, "Optimal design of lcl harmonic filters for three-phase pfc rectifiers," *IEEE Trans. Power Electron.*, vol. 28, no. 7, pp. 3114–3125, 2013.

[6] K. B. Park, F. D. Kieferndorf, U. Drofenik, S. Pettersson, and F. Canales, "Weight Minimization of LCL Filters for High-Power Converters: Impact of PWM Method on Power Loss and Power Density," *IEEE Trans. Ind. Appl.*, vol. 53, no. 3, pp. 2282–2296, 2017.

[7] J. Mühlethaler, "Modeling and multi-objective optimization of inductive power components," no. 20217, 2012. [Online]. Available: http://e-collection.library.ethz.ch/view/eth:5781

[8] J. A. Ferreira, "Improved Analytical Modeling of Conductive Losses in Magnetic Components," *IEEE Trans. Power Electron.*, vol. 9, no. 1, pp. 127–131, 1994.

[9] D. G. Holmes and T. A. Lipo, "Pulse Width Modulation for Power Converters: Principles and Practice," *Pulse Width Modul. Power Convert.*, pp. 531–554.

[10] Y. Wu, A. Shekhar, T. B. Soeiro, and P. Bauer, "Voltage Source Converter Control under Distorted Grid Voltage for Hybrid AC-DC Distribution Links," *IECON 2019 - 45th Annu. Conf. IEEE Ind. Electron. Soc.*, vol. 1, pp. 5694–5699, 2019.

[11] Chang Sung Powder Core Material. [Online]. Available: http://www.changsung.com/_eng/index.php

[12] P. Dowell, "Effects of eddy currents in transformer windings," *Proc. Inst. Electr. Eng.*, vol. 113, no. 8, p. 1387, 1966.

[13] J. Reinert, A. Brockmeyer, and R. W. De Doncker, "Calculation of losses in ferro- and ferrimagnetic materials based on the modified Steinmetz equation," *IEEE Trans. Ind. Appl.*, vol. 37, no. 4, pp. 1055–1061, 2001.

[14] Semikron, "Semikron IGBT Modules." [Online]. Available: https://www.semikron.com/products/product-classes/igbt-modules.html